Steric control of supramolecular association in structures of $Zn(S_2COR)_2$ with *N*,*N*′-bis(pyridin-4-ylmethyl)oxalamide

Yee Seng Tan[I], Hao Zhe Chun,[I,II] Mukesh M. Jotani[III] and Edward R. T. Tiekink[*I]

[I] Centre for Crystalline Materials, Faculty of Science and Technology, Sunway University, 47500 Bandar Sunway, Selangor Darul Ehsan, Malaysia

[II] Department of Materials Science and Metallurgy, University of Cambridge, 27 Charles Babbage Road, Cambridge CB3 0FS, United Kingdom

[III] Department of Physics, Bhavan's Sheth R. A. College of Science, Ahmedabad, Gujarat 380001, India

Received; accepted

Keywords: Zinc xanthate / coordination polymer / hydrogen bonding / Hirshfeld surface / crystal structure analysis / X-ray diffraction

Abstract. The crystal and molecular structures of the one-dimensional coordination polymer $[Zn(S_2COEt)_2(^4LH_2)]_n$ (**1**) and binuclear $[Zn(S_2COCy)_2]_2(^4LH_2)$ (**2**) are described, where $^4LH_2$ is N,N'-bis(pyridin-4-ylmethyl)ethanediamide. In **1**, the $Zn(S_2COEt)_2$ entities are linked by bidentate bridging $^4LH_2$ ligands through the pyridyl-N atoms to generate a twisted supramolecular chain. As a result of monodentate xanthate ligands, the N_2S_4 donor set defines a distorted tetrahedral coordination geometry and, crucially, allows the participation of the non-coordinating sulphur atoms in supramolecular association. Thus, in the crystal amide-N–H···O(amide) and amide-N–H···S(thione) hydrogen bonds link chains into a three-dimensional architecture. The substitution of the ethyl group in the xanthate ligand with a cyclohexyl group results in very different structural outcomes. In **2**, a binuclear molecule is observed with the coordination geometry for zinc being defined by chelating xanthate ligands and a pyridyl-N atom with the NS_4 donor set defining a highly distorted geometry. In the molecular packing, amide-N–H···S(thione) hydrogen bonds stabilise a supramolecular chain along the a-axis and these are connected into a three-dimensional arrangement by methylene-C–H···O and methylene-C–H···π(pyridyl) interactions. The relative importance of the specified intermolecular interactions and weaker, contributing contacts has been revealed by an analysis of the Hirshfeld surfaces of **1** and **2**.

[*] Correspondence authors: mmjotani@rediffmail.com (M.M.J.); edwardt@sunway.edu.my (E.R.T.T.)

Introduction

The structural chemistry of metal dithiocarbamates ($^{-}S_2CNRR'$) [1,2] is significantly more developed compared with that of other 1,1-dithiolate ligands, with those of the metal dithiophosphates [$^{-}S_2P(OR)(OR')$] [3] and metal xanthates ($^{-}S_2COR$) [4] being the next most advanced, R, R' = alkyl, aryl. Of particular relevance to the present report are the structures of the zinc 1,1-dithiolates where μ_2-bridging modes of coordination of the 1,1-dithiolate ligand are often found [5]. In the dithiocarbamates, binuclear $\{Zn[S_2CN(R)R']_2\}_2$ aggregates are usually observed owing to equal numbers of bridging and chelating ligands. Similar binuclear aggregates are observed in the dithiophosphates but, one-dimensional coordination polymers are also known. The structural chemistry of the binary zinc xanthates is considerably more diverse, featuring zero-dimensional (tetranuclear), one-dimensional (chains) and two-dimensional (layers) aggregation patterns [5]. Crucially, steric control is suggested as being largely responsible for mitigating aggregation in the solid-state, i.e. increasing the size of R/R' reduces the dimension of the aggregate [5-7]. This is nicely illustrated for the aforementioned xanthate structures where decreasing aggregation is correlated with the greater bulk of the substituent, i.e. R = Et (layer), *n*-Pr (chain) and *i*-Pr (tetramer) [8].

The structural chemistry of the zinc-triad 1,1-dithiolates with potentially bridging bipyridyl-type ligands, i.e. N∩N, has been reviewed recently [9]. This chemistry is varied, often leading to unexpected reaction outcomes, in terms of stoichiometry, and a monodentate coordination mode for what might be expected to be bidentate bridging molecules, especially in the presence of hydrogen bonding functionality in the 1,1-dithiolate ligands [9]. For example, regardless of the stoichiometry of the reagents in the reaction between $Cd[S_2CN(i\text{-}Pr)CH_2CH_2OH]_2$ and trans-1,2-bis(4-bipyridyl)ethylene (bpe), i.e. 2:1, 1:1 and 1:2, only the 2:3 species, $\{Cd[S_2CN(i\text{-}Pr)CH_2CH_2OH]_2\}_2(bpe)_3$, could be isolated [10]. This species contains rare examples of monodentate coordination for the bpe ligands and the terminal, non-bonding pyridyl-nitrogen atoms of the bpe ligands form hydrogen bonding interactions instead. Even in examples where hydrogen bonding is not possible, excess N∩N reagent does not necessarily lead to increased coordination numbers and/or bridging, rather monodentate coordination as in $Zn[S_2CN(n\text{-}Pr)_2]_2(bpy)$ [11] or the incorporation of non-coordinating bpe molecules in the crystal, e.g. in the lattice adduct $[Zn(S_2CNEt_2)_2]_2(bpe)\cdot bpe$ [12]; bpy = 4,4'-bipyridyl. For adducts of zinc xanthates, particularly relevant to the present investigation, a variety of structural motifs have been found, i.e. zero-dimensional binuclear $[Zn(S_2CO\text{-}i\text{-}Pr)_2]_2(pyrazine)$ [13], $[Zn(S_2CO\text{-}i\text{-}Pr)_2]_2(bpy)$ [14] and $[Zn(S_2COCy)_2]_2(bpe)$ [15]. One-dimensional coordination polymers have also been observed with linear, i.e. $\{[Zn(S_2CO\text{-}i\text{-}Pr)_2]_2(pyrazine)\}_n$ [16], helical, i.e. $\{[Zn(S_2CO\text{-}i\text{-}Bu)_2]_2(bpy)\}_n$ [17], and zig-zag topologies, i.e. $\{[Zn(S_2COR)_2]_2(bpe)\}_n$ for R = Et and *n*-Bu [15]. In an attempt to increase the dimensionality of the supramolecular aggregation in N∩N adducts of $Zn(S_2COR)_2$, hydrogen bonding functionality has been incorporated into the N∩N ligand, i.e. a diamide link as in N,N'-bis(pyridin-4-ylmethyl)ethanediamide ($^4LH_2$), as shown in Figure 1.

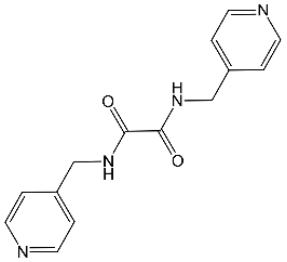

Fig. 1: Structural formula for the bridging ligand, $^4LH_2$, in each of **1** and **2**.

The structural chemistry of the isomeric N,N'-bis(pyridin-n-ylmethyl)ethanediamides, $^{n}LH_2$ for n = 2, 3 and 4, has also been reviewed in recent times [18]. With potential for supramolecular aggregation via hydrogen [19] and halogen [20] bonding, often leading to two-dimensional arrays, these molecules featured prominently in the pioneering days of crystal engineering. The neutral molecules, i.e. $^{3}LH_2$ and $^{4}LH_2$, are effective ligands for metals, coordinating via the pyridyl-nitrogen atoms, potentially leading to coordination polymers, with additional supramolecular association occurring via hydrogen bonding interactions involving the diamide residue. A nice example of this is found in the crystal of $I_2Hg(^{4}LH_2)HgI_2$ whereby two HgI_2 units are linked via a bidentate $^{4}LH_2$ ligand, with these binuclear residues linked into a supramolecular chain via amide-N–H···O(amide) hydrogen bonds through 10-membered $\{\cdots HNCCO\}_2$ synthons [21]. In terms of adducts with the zinc-triad 1,1-dithiolates, some interesting structures have been characterised starting with interwoven, linear coordination polymers [22]. Here, binuclear $\{Zn[S_2CN(Me)CH_2CH_2OH]_2\}_2(^{3}LH_2)$ species are linked into a supramolecular chain via hydroxyl-O–H···O(hydroxyl) hydrogen bonds. Two of these are interwoven to form a doubly interconnected chain, being linked by hydroxyl-O–H···O(carbonyl) hydrogen bonds [22]. The analogous chemistry with $[Zn(S_2CNR_2)]_2(^{3}LH_2)$ gives quite distinct results [23]: for the R = Me compound, solvent dimethylformamide molecules hydrogen bond to the diamide moiety precluding further supramolecular aggregation but, in the R = *n*-Pr structure, supramolecular chains are formed as described above for $I_2Hg(^{4}LH_2)HgI_2$ [21]. A recent study of binuclear $[Zn(S_2CNEt_2)]_2(^{4}LH_2)$ again showed no conventional hydrogen bonding [24]. It was in connection of the latter studies that attention was directed to investigation the structural chemistry of zinc xanthates with $^{4}LH_2$, especially as $Zn(S_2COR)_2$ compounds show a greater propensity for supramolecular aggregation (see above). Herein, the crystal and molecular structures of two species, coordination polymer $[Zn(S_2COEt)_2(^{4}LH_2)]_n$ (**1**) and binuclear $[Zn(S_2COCy)_2]_2(^{4}LH_2)$ (**2**), are described along with an analysis of their calculated Hirshfeld surfaces.

Experimental

Instrumentation

Elemental analyses were performed on a LECO TruSpec® Micro CHN analyser. IR spectra were obtained on a Bruker Vertex 70 V spectrophotometer equipped with a Platinum ATR. ^{1}H and $^{13}C\{^{1}H\}$ NMR spectra were recorded in DMSO-d_6 solution on a Bruker Ascend 400 MHz NMR spectrometer with chemical shifts relative to tetramethylsilane.

Materials

The $Zn(S_2COEt)_2$ and $Zn(S_2COCy)_2$ reagents were prepared in high yield from the 1:2 reaction of $ZnCl_2$ and $K[S_2COR]$ (R = Et or Cy) in distilled water following established procedures [25]. The *N*,*N'*-bis(4-pyridylmethyl)oxalamide reagent was prepared in high yield from refluxing 4-picolylamine (Aldrich) and diethyl oxalate (Sigma-Aldrich), in a 2:1 mole ratio, in ethanol solution [15].

Synthesis

$[Zn(S_2COEt)_2(^{4}LH_2)]_n$ (**1**): *N*,*N'*-bis(4-pyridylmethyl)oxalamide (0.09 g, 0.33 mmol) in ethanol/acetonitrile (20 ml, v/v 1:1) was added slowly to $Zn(S_2COEt)_2$ (0.20 g, 0.65 mmol) also dissolved in ethanol/acetonitrile (20

ml, v/v 1:1). The resulting mixture was stirred for 30 mins at 323 K, followed by filtration. The filtrate was left for slow evaporation under ambient conditions. Colourless crystals formed after three weeks. Yield: 0.07 g (18.6%) (based on Zn). Anal. Calcd for $C_{20}H_{24}N_4O_4S_4Zn$: C 41.55; H 4.18; N 9.69. Found: C 41.92; H 4.48; N 9.72. IR (cm^{-1}): 3366 (w) (N–H); 1664 (s) (C=O); 1176(s) (C–O); 1031 (s) (C–S). ^{1}H NMR (DMSO-d_6): 9.49 (*t*, 2H, NH, J_{HH} = 6.32 Hz), 8.52 (*d*, 4H, aryl-NCH, J_{HH} = 5.88 Hz), 7.34 (*d*, 4H, aryl-CH, J_{HH} = 5.64 Hz), 4.40 (*d*, 4H, CH_2, J_{HH} = 6.36 Hz), 4.33 (*q*, 4H, OCH_2, J_{HH} = 7.11 Hz), 1.22 (*t*, 6H, CH_3, J_{HH} = 7.08 Hz) ppm. ^{13}C{^{1}H} NMR (DMSO-d_6): 160.5 (C=O), 149.8 (N<u>C</u>H), 149.0 (aryl-C_{ipso}), 123.0 (aryl-<u>C</u>H), 70.2 (OCH_2), 42.0 (CH_2), 14.3 (CH_3) ppm; not observed: $C_{quaternary}$.

[Zn($S_2COCy)_2]_2(^4LH_2$) (**2**): The compound was prepared and recrystallised as for **1** through the reaction of *N*,*N'*-bis(4-pyridylmethyl)oxalamide (0.13g, 0.48 mmol) and Zn($S_2COCy)_2$ (0.20 g, 0.48 mmol). Yield: 0.0042 g (1.59 %) (based on Zn). Anal. Calcd for $C_{42}H_{58}N_4O_6S_8Zn_2$: C 45.77; H 5.30; N 5.08. Found: C 45.79; H 5.28; N 4.95. IR (cm^{-1}): 3300 (w) (N–H); 1682 (s) (C=O); 1150 (m) (C–O); 1029 (m) (C–S). ^{1}H NMR (DMSO-d_6): 9.47 (*t*, 2H, NH, J_{HH} = 6.34 Hz), 8.51 (*d*, 4H, aryl-NCH, J_{HH} = 3.08 Hz), 7.29 (*d*, 4H, aryl-CH, J_{HH} = 4.68 Hz), 5.10 (*m*, 4H, CH, J_{HH} = 4.25 Hz), 4.38 (*d*, 4H, CH_2, J_{HH} = 6.36 Hz), 1.91-1.20 (*m*, 40H, Cy) ppm. ^{13}C{1H} NMR {DMSO-d_6}: 160.7 (C=O), 149.9 (N<u>C</u>H), 148.3 (aryl-C_{ipso}) 122.8 (aryl-<u>C</u>H), 82.8 (OCH), 42.0 (CH_2), 31.2 (Cy-C_{ortho}), 25.3 (Cy-C_{para}), 23.8 (Cy-C_{meta}) ppm; not observed: $C_{quaternary}$.

Crystal structure determination

Intensity data for **1** and **2** were measured at 100 K on a Rigaku/Oxford Diffraction XtaLAB Synergy diffractometer (Dualflex, AtlasS2) fitted with CuKα radiation (λ = 1.54178 Å) so that θ_{max} = 67.1°. Data processing and gaussian absorption corrections were accomplished with CrysAlis Pro [26]. Details of cell data, X-ray data collection, and structure refinement are given in Table 1. The structures were solved by Direct Methods [27]. Full-matrix least squares refinement on F^2 with anisotropic displacement parameters for all non-hydrogen atoms was performed [28]. The C-bound H atoms were placed on stereochemical grounds and refined with fixed geometries, each riding on a carrier atom with U_{iso} = 1.2-1.5U_{equiv}(carrier atom). The N-bound H atoms were found in difference maps and refined with N–H = 0.88±0.01 Å, and with U_{iso} = 1.2U_{eq}(N). A weighting scheme of the form $w = 1/[\sigma^2(F_o^2) + (aP)^2 + bP]$ where $P = (F_o^2 + 2F_c^2)/3$ was introduced in each case. In the refinement of **1**, three reflections, i.e. (-3 5 13), (8 8 0) and (9 3 9), were omitted from the final cycles of refinement owing to poor agreement; in **2**, one reflection, i.e. (1 1 5), was omitted for the same reason. The programs WinGX [29], ORTEP-3 for Windows [29] and PLATON [30] and DIAMOND [31] were also used in the study.

Tab. 1: Crystallographic data and refinement details for **1** and **2**.[1]

	1	**2**
Formula	$C_{20}H_{24}N_4O_4S_4Zn$	$C_{42}H_{58}N_4O_6S_8Zn_2$
Formula weight	578.04	1102.14
Crystal colour, habit	Colourless, prism	Colourless, prism
Crystal size/mm	0.06 x 0.11 x 0.14	0.06 x 0.08 x 0.11
Crystal system	monoclinic	monoclinic
Space group	$P2_1/c$	$P2_1/n$
a/Å	11.6624(2)	9.86560(10)
b/Å	9.26290(10)	11.03440(10)

c/Å	23.3053(4)	22.7417(2)
β/°	98.835(2)	91.2600(10)
V/Å^3	2487.74(7)	2475.09(4)
Z/Z'	4/1	2/0.5
D_c/g cm^{-3}	1.543	1.479
F(000)	1192	1148
μ(Cu $K\alpha$)/mm^{-1}	4.806	4.741
Measured data	27317	27330
θ range/°	3.8 – 67.1	3.9 – 67.1
Unique data	4426	4407
R_{int}	0.030	0.045
Observed data ($I \geq 2.0\sigma(I)$)	4085	4012
R, obs. data; all data	0.030; 0.033	0.037; 0.041
a; b in wghting scheme	0.040; 3.488	0.081; 1.678
R_w, obs. data; all data	0.077; 0.079	0.112; 0.116
Largest difference peaks (Å^{-3})	0.63, -0.41	0.99, -0.70

[1] Supplementary Material: Crystallographic data (including structure factors) for the structures reported in this paper have been deposited with the Cambridge Crystallographic Data Centre as supplementary publication numbers CCDC-1846506 and 1846505. Copies of available material can be obtained free of charge, on application to CCDC, 12 Union Road, Cambridge CB2 1EZ, UK, (fax: +44-(0)1223-336033 or e-mail: deposit@ccdc.cam.ac.uk).

Results and discussion

Molecular structures

The crystallographic asymmetric unit of **1** is shown in Figure 2 and comprises $Zn(S_2COEt)_2$ and two half molecules of $^4LH_2$, as each of the latter is disposed about a centre of inversion. Selected bond lengths are collected in Table 2. The zinc centre is coordinated by two xanthate ligands which adopt the comparatively rare coordination mode [3] whereby one sulphur atom is coordinated and the oxygen atom, rather than the thione-sulphur atom, is directed towards the metal centre. The Zn···O1 separation for the S1-xanthate ligand of 2.8154(16) Å is nearly 1 Å less than the sum of the van der Waals radii of zinc and sulphur of 3.77 Å [32]. The comparable Zn···O2 separation for the S3-xanthate ligand is considerably longer at 3.2194(16) Å, being about 0.5 Å shorter than the sum of the respective van der Waals radii. A direct result of the adopted coordination mode is a significant disparity in the associated C–S bond lengths, with sulphur atoms forming the bonds to zinc having considerably longer C–S bonds, by up to 0.07 Å, than the comparable bonds formed by the thione-S atoms, Table 2. The four-coordinate geometry for zinc is completed by two pyridyl-N atoms derived from two $^4LH_2$ ligands. The coordination geometry is based on a N_2S_2 tetrahedron with the minimum angle of 103.03(5)° found for S1–Zn–N3 and the maximum angle being 117.38(5)° for S1–Zn–N1. The minimal distortions from ideal tetrahedral geometry is reflected in the value of τ_4 = 0.89, a geometric descriptor for four-coordinate geometries [33], which compares to 1.0 for an ideal tetrahedron and 0.0 for an ideal square plane, and emphasises the weak nature of the intramolecular Zn···O contacts.

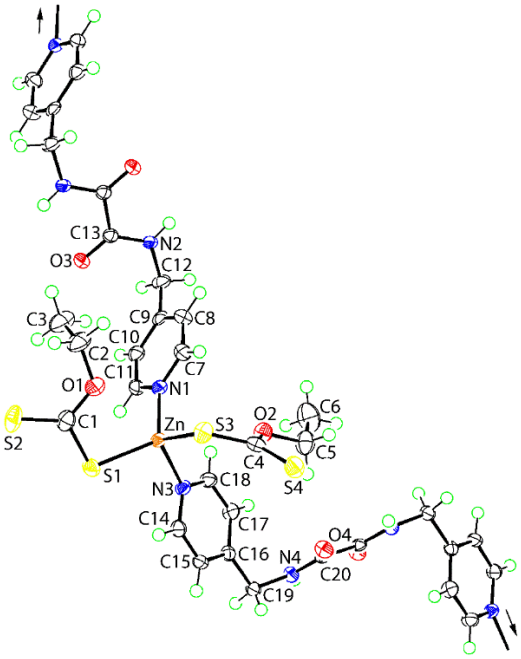

Fig. 2: The asymmetric unit of **1** expanded to show the full N1- and N3-ligand molecules, each of which is disposed about a centre of inversion. The unlabelled atoms for the N1- and N3-ligand molecules are related by symmetry operations -*x*, 2-*y*, -*z* and 1-*x*, 1-*y*, 1-*z*, respectively. Displacement ellipsoids are drawn at the 70% probability level.

Tab. 2: Selected bond lengths (Å) for **1** and **2**.[a]

	1 (x = 4)	**2** (x = 8)
Zn–S1	2.3016(6)	2.3168(6)
Zn–S2	–	2.7266(6)
Zn···O1	2.8154(16)	–
Zn–S3	2.3116(6)	2.3569(6)
Zn–S4	–	2.5164(7)
Zn···O2	3.2194(16)	–
Zn–N1	2.0265(18)	2.032(2)
Zn–N3	2.0471(18)	–
C1–S1, S2	1.715(2), 1.650(2)	1.713(2), 1.686(2)
C(x)–S3, S4	1.728(2), 1.652(2)	1.714(3), 1.693(3)
amide-C–C(amide)	1.531(4); 1.532(4)	1.544(5)

a The "x" refers to the number in C(x).

In the bridging $^4LH_2$ molecule, intramolecular amide-N–H···O(amide) hydrogen bonds are noted, Table 3. These interactions probably contribute to the planarity of the planar central residue comprising the amide-O, N and C atoms as well as the appended methylene-C atom which exhibit a r.m.s. deviation of 0.007 Å [0.005 Å for the O4-amide]. This plane forms a dihedral angle of 84.24(6)° with the 4-pyridyl ligand [72.76(6)° for the O4-amide]. Overall, each $^4LH_2$ molecule has an anti-periplanar conformation as is found in the two polymorphs of the uncoordinated molecule [34,35]. Finally, it is noted the central amide-C–C(amide) bond lengths (Table 2) are longer than usually anticipated C(sp^2)–C(sp^2) bonds, an observation related to the presence of electronegative groups bound to these atoms, as discussed in the literature [18].

Tab. 3: Summary of intermolecular interactions (A–H···B; Å, º) operating in the crystals of **1** and **2**.

A	H	B	A–H	H···B	A···B	A–H···B	Symmetry operation
1							
N2	H2n	O3	0.869(17)	2.39(2)	2.716(2)	102.6(15)	1-*x*, 1-*y*, 1-*z*
N4	H4n	O4	0.87(2)	2.317(19)	2.696(2)	106.5(16)	-*x*, 2-*y*, -*z*
N2	H2n	S4	0.869(17)	2.877(18)	3.6079(19)	142.8(14)	1-*x*, ½+*y*, ½-*z*
N4	H4n	O3	0.87(2)	2.22(2)	2.882(2)	133.0(17)	-*x*, ½+*y*, ½-*z*
2							
N2	H2n	O3	0.88(2)	2.32(3)	2.710(3)	106.7(18)	2-*x*, -*y*, -*z*
N2	H2n	S2	0.88(2)	2.54(2)	3.306(2)	147(2)	1+*x*, *y*, *z*
C4	H4a	O3	0.99	2.52	3.410(4)	150	1-*x*, -*y*, -*z*
C12	H12b	O3	0.99	2.57	3.356(3)	136	½-*x*, ½+*y*, ½-*z*
C7	H7b	Cg(N1,C15-C19)	0.99	2.68	3.543(3)	146	1-*x*, 1-*y*, -*z*

As each of the $^4LH_2$ molecules is bidentate bridging, a coordination polymer is generated, Figure 3. With the aforementioned anti-periplanar conformations, the topology of the chain, propagated approximately along [1 $\bar{1}$ 6], is twisted.

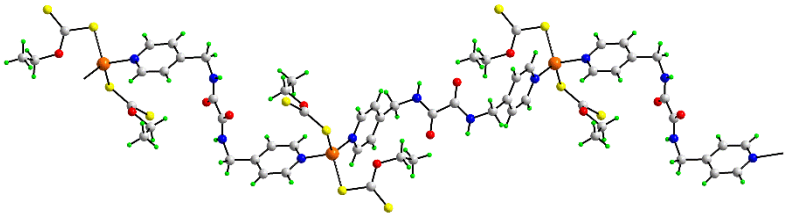

Fig. 3: The one-dimensional coordination polymer in the crystal of **1**.

The crystallographic asymmetric unit of **2** comprises $Zn(S_2COCy)_2$ and half a $^4LH_2$ molecule, as this is disposed about a centre of inversion. The application of symmetry leads to a zero-dimensional binuclear molecule as shown in Figure 4; geometric parameters are given in Table 2. The S1-xanthate ligand coordinates in an asymmetric S, S mode with the difference between the Zn–S1, S2 bond lengths being 0.41 Å. The S3-xanthate ligand coordinates more symmetrically with the difference in the Zn–S3, S4 bond lengths being only 0.16 Å. As a consequence of this, the difference in the C–S bond lengths is reduced to approximately 0.02 Å, cf. to the disparity seen in **1** (Table 2). The NS_4 coordination geometry is highly distorted with angles ranging from a small, 71.40(2)°, for the S1–Zn–S2 chelate angle to 165.00(2)°, for S2–Zn–S4, i.e. involving the weakly bound sulphur atoms. The value of τ, a descriptor for five-coordinate geometries [36], computes to 0.64, which compares to 0.0 and 1.0 for ideal square-pyramidal and trigonal-bipyramidal geometries, respectively.

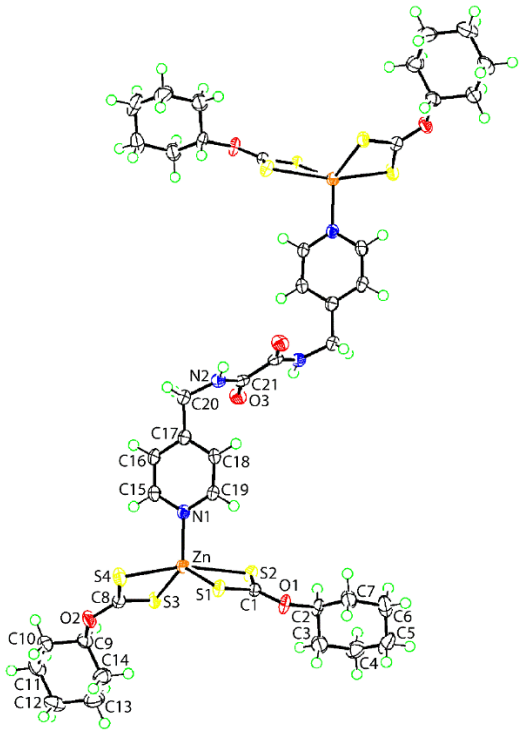

Fig. 4: Molecular structure of **2**. The molecule is disposed about a centre of inversion with unlabelled atoms related by symmetry operation 2-*x*, -*y*, -*z*. Displacement ellipsoids are drawn at the 70% probability level.

As for **1**, the centrosymmetric $^4LH_2$ molecule in **2** has an anti-periplanar conformation, features intramolecular amide-N–H···O(amide) hydrogen bonds (Table 3), a planar central C_2NO residue [r.m.s. deviation = 0.014 Å] and an almost perpendicular relationship between the central plane and that through the 4-pyridyl ring [dihedral angle = 80.47(7)°].

The different molecular structures observed for **1** and **2** are readily rationalised in terms of the steric bulk of the oxygen-bound R groups in the xanthate ligands. In short, the larger cyclohexyl group in **2** precludes the formation of a coordination polymer. Such considerations are well-established in the structural chemistry of metal 1,1-dithiolates [5-8], including in coordination polymers mediated by bridging bipyridyl-type ligands where both polymer formation and topology can be controlled by tailoring the steric bulk of the R substituents and positioning of the pyridyl-nitrogen atoms [9,37-39]. Indeed, there are two direct precedents for **1** and **2** in the crystallographic literature, namely $[Zn(S_2COEt)_2(bpe)]_n$ and binuclear $[Zn(S_2COCy)_2]_2(bpe)$ [15]. In this study, different solid-state luminescence responses were ascribed to the different modes of association between $Zn(S_2COR)_2$ residues based on molecular orbital calculations [15]. In the present and previous [15] studies, only binuclear species were isolated, i.e. **2** and $[Zn(S_2COCy)_2]_2(bpe)$, respectively, regardless of the stoichiometry of the reagents. Further, the electronic structures, as determined by density functional theory calculations do not differ significantly [40]. The difference between the two pairs of structures rests in the hydrogen bonding potential of the bridging ligands in **1** and **2**, details of which are presented below in "Molecular Packing".

Molecular packing

The molecular packing of **1** features conventional amide-N–H···O(amide) hydrogen bonding so that the amide-N–H groups of a N3-$^4LH_2$ ligand form hydrogen bonds to the amide-O3 atoms of a N1-$^4LH_2$ ligand to form linear chains along [1 0 0]. The amide-N–H groups of the N1-$^4LH_2$ ligand form amide-N–H···S(thione) hydrogen bonds with non-coordinating S4 atoms. The result of these interactions is the linking of the supramolecular polymers into a three-dimensional architecture, Figure 5. While no hydrogen bonding role is apparent for the amide-O4 atom, this forms a close C–H···O contact as discussed below in the description of the Hirshfeld surfaces calculated for **1** and **2**. It is noted that the deviations from linearity of the specified intermolecular hydrogen bonds are a result of the presence of intramolecular amine-N–H···O(amide) hydrogen bonds.

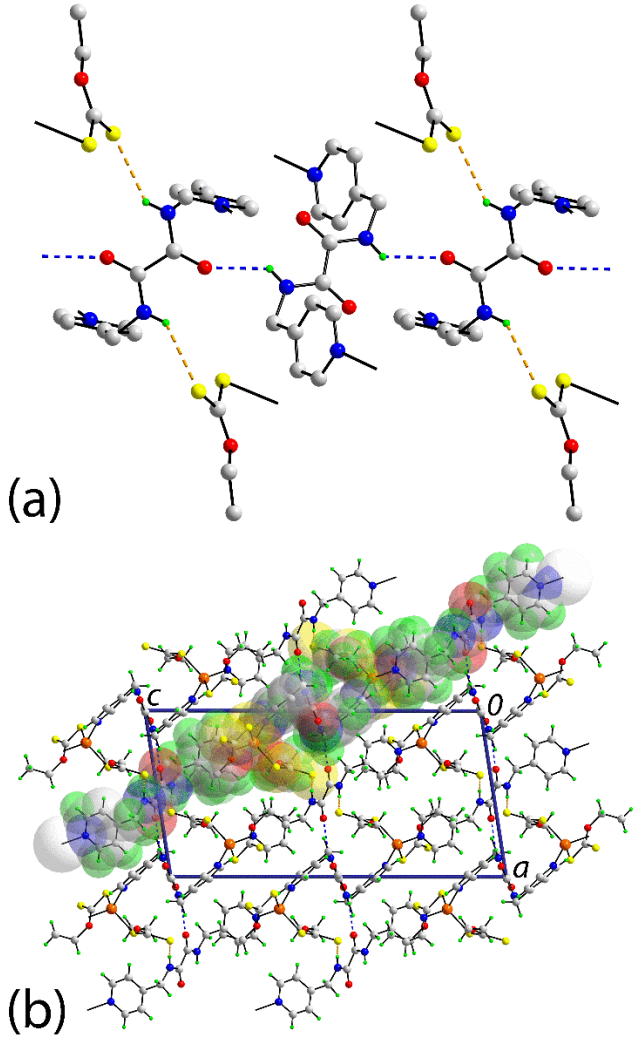

Fig. 5: Molecular packing in **1**: (**a**) detail of the hydrogen bonding with non-participating hydrogen atoms omitted as are pendant residues and (**b**) a view of the unit cell contents shown in projection down the *b*-axis; one supramolecular polymer is highlighted in space-filling mode. The amide-N–H···O(amide) and amide-N–H···S(thione) hydrogen bonds are shown as blue and orange dashed lines respectively.

The molecular packing of **2** is devoid of amide-N–H···O(amide) hydrogen bonding but, features amide-N–H···S(thione) hydrogen bonds, Table 2. As illustrated in Figure 6a, this hydrogen bonding results in the formation of centrosymmetric, 24-membered $\{\cdots HNC_2NC_4NZnS\}_2$ synthons that stabilise a supramolecular chain along [1 0 0]. The amide-O3 atom accepts an interaction from a methylene-C4–H atom to contribute to the stabilisation of the chain. The amide-O3 atom also participates in a methylene-C12–H···O3(amide) interaction to connect chains along [0 0 1]. Finally, methylene-C7–H···π(pyridyl) provide connections along [0 1 0] to consolidate the three-dimensional packing, Figure 6b.

In neither crystal were supramolecular amide tapes sustained by 10-membered $\{\cdots HNCCO\}_2$ synthons observed. This, despite tapes are sometimes seen in other metal salts, but usually in cases where the metal centres are relatively sterically unencumbered, e.g. metal halides [21,41], and often in co-crystals [20,25,42,43]. In **1**, chains were formed by amide-N–H···O(amide) hydrogen bonds with additional amide-N–H hydrogen bonds involving thione-S atoms. In **2**, chains are also formed but, sustained by amide-N–H hydrogen bonds exclusively, as detailed above. In both cases, the amide-oxygen atoms did not participate in conventional hydrogen

bonding interactions but, participated in C–H···O(amide) interactions instead. Given that supramolecular amide tapes are not formed in either **1** or **2**, it is likely that the steric bulk of the zinc atom environments preclude the close approach necessary for their formation. It is also possible that the relatively electronegative sulphur atoms provide a measure of competition for hydrogen bonding interactions [44-46].

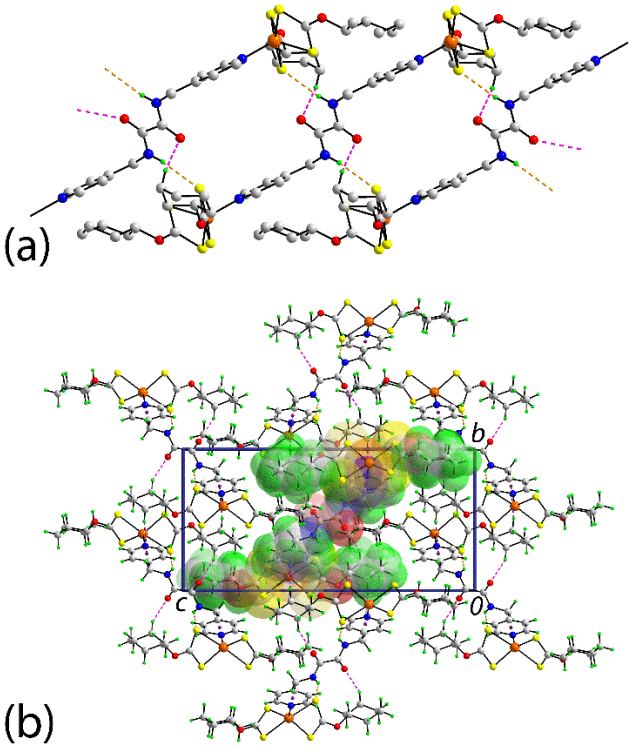

Fig. 6: Molecular packing in **2**: (**a**) detail of the supramolecular chain along [1 0 0] with N–H···S and C–H···O interactions shown as orange and pink dashed lines, respectively; non-participating hydrogen atoms have been omitted and (**b**) view of the unit cell contents shown in projection down the *a*-axis with one supramolecular chain highlighted in space-filling mode. The C–H···π interactions are indicated by purple dashed lines.

Hirshfeld surface analysis

The Hirshfeld surface calculations [47,48] were performed in accord with recent studies on related zinc-triad dithiocarbamate structures [49,50] in order to gain a greater understanding of the molecular packing in **1** and **2**.

On the Hirshfeld surface mapped over d_{norm} for **1**, Figures 7a and b, and for **2**, Figure 7c, the conventional N–H···O and N–H···S hydrogen bonds (Table 3) are evident from broad and bright-red spots near the participating atoms. In addition, the bright-red spot near the S4 atom in **1**, Figure 7b, indicates the significant influence of the short interatomic S···S contact (Table 4) on the packing. The presence of comparatively weak intermolecular C–H···S and C–H···O interactions (Table 5) in the crystal of **1** results in diminutive-red spots near respective atoms in Figures 7a and b. The short interatomic contacts summarised in Table 4 also result in faint-red spots in Figure 7. Finally, for **1**, the broad-red spots appearing near the N1 and N3 atoms of the $^4LH_2$ ligand, indicated by thick arrows in Figure 7a. are a result of the formation of the polymeric chain. On the Hirshfeld surface mapped over d_{norm} for binuclear **2**, the intermolecular methylene-C4–H4a···O3(amide) and methylene-C12–H12b···O3(amide) contacts (Table 3) are viewed as bright-red and tiny-red spots, respectively, near the donor-acceptor atom

pairs on the surface, Figure 7c. The other faint-red spots seen in Figure 7c are indicative of the short interatomic contacts summarised in Table 4.

Tab. 4: Additional short contacts (Å) in **1** and **2**.

Contact	Distance (Å)	Symmetry Operation
1		
S4···S4	3.219(1)	1 - *x*, 1 - *y*, -*z*
S2···C9	3.472(2)	- *x*, 1 + *y*, *z*
S2···C10	3.432(2)	- *x*, 1 + *y*, *z*
S4···C19	3.482(2)	- *x*, 1 - *y*, 1 - *z*
S4···H3a	2. 877(2)	1 - *x*, ½ + *y*, ½ - *z*
S4···H19b	2.90	- *x*, 1 - *y*, 1 - *z*
2		
C19···O1	3.137(3)	1 - *x*, - *y*, 2 - *z*
S1···H4b	2.83	- *x*, 1 - *y*, - *z*
S1···H19	2.83	1 - *x*, 1 - *y*, - *z*
S2···H10a	2.84	½ - *x*, -½ + *y*, ½ - *z*

The donors and acceptors of intermolecular interactions in coordination polymer **1** and binuclear species **2** are viewed as blue and red regions corresponding to positive and negative electrostatic potentials on the Hirshfeld surfaces mapped over electrostatic potential in Figure 8. The influence of intramolecular C–H···π and intermolecular C–S···π interactions in the crystal of **1** (Table 5) are illustrated on the Hirshfeld surface mapped with the shape-index property in Figure 9a. Similarly, the intramolecular C–H···π contact in **2** (Table 5) is highlighted in Figures 9b and c. The interesting feature of the π-system in the latter contact is that it is defined by the chelate ring defined by the xanthate ligand. This arises as the resonance structure with a formal negative charge on each sulphur atom, i.e. $^{2-}S_2C{=}O^{+}R$, contributes about 20% to the overall electronic structure meaning the chelate ring is both aromatic and electron-rich, serves as an efficient acceptor for end-on C–H···π interactions and provide energies of stabilisation akin to intermolecular M···S secondary bonding interactions [7,51].

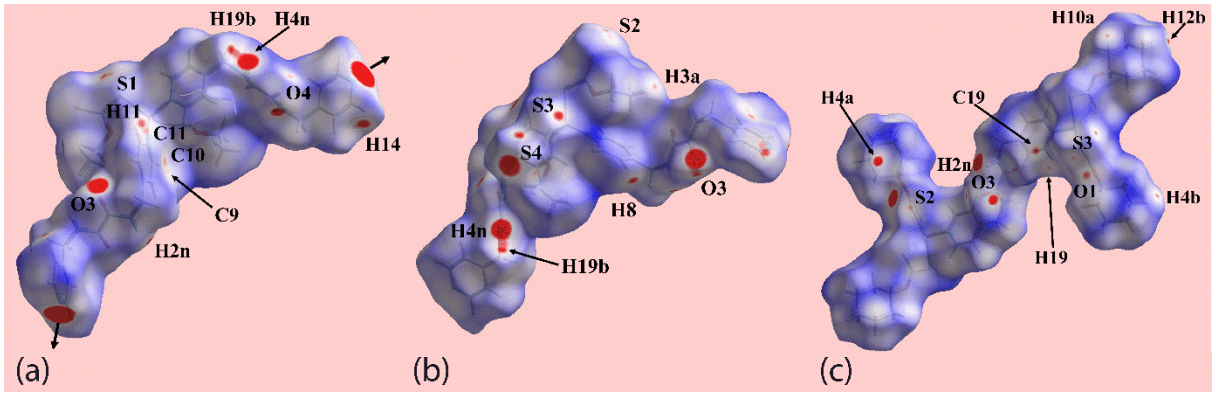

Fig. 7: Views of Hirshfeld surfaces mapped over d_{norm} for (a) and (b) **1**, mapped over the range -0.089 to +1.496 atomic units (a.u.), and (c) **2**, mapped over the range -0.085 to + 1.529 a.u. The brightest spots correlate with the most significant intermolecular interactions.

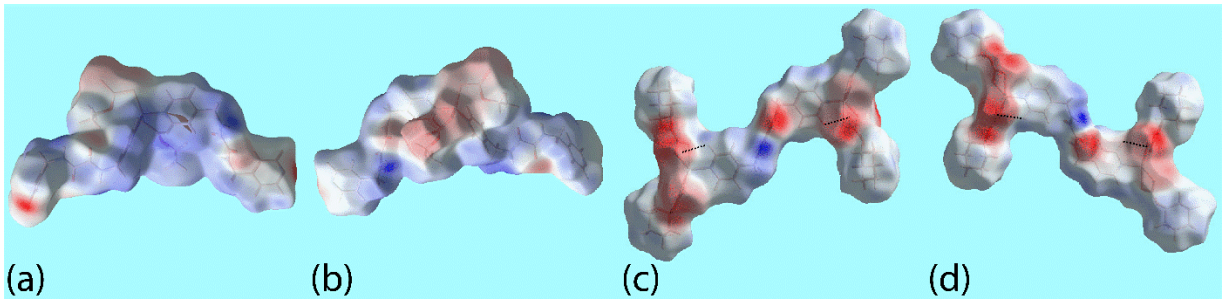

Fig. 8: Views of the Hirshfeld surfaces mapped over the electrostatic potential for (a) and (b) **1**, mapped over the range -0.114 to + 0.098 a.u., and (c) and (d) **2**, mapped over the range -0.057 to + 0.072 a.u. The intramolecular C–H···π interactions are shown with black dotted lines. The red and blue regions represent negative and positive electrostatic potentials, respectively.

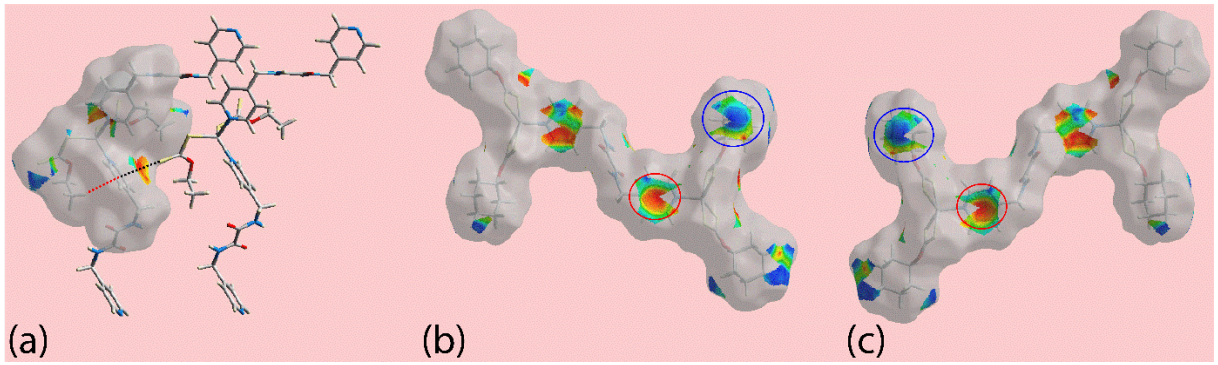

Fig. 9: Views of the Hirshfeld surfaces mapped with the shape-index property for (a) **1**, highlighting intramolecular C–H···π and intermolecular C–S···π interactions by red and black dotted lines, respectively, and (b) and (c) **2**, highlighting donors and acceptors of the C–H···π interactions within blue and red circles, respectively.

Tab. 5: Additional intermolecular interactions (A–X···B; Å, º) operating in the crystals of **1** and **2**.

A	X	B	A–X	H···B	A···B	A–H···B	Symmetry operation
1							
C8	H8	S3	0.85	2.87	3.768(3)		*x*, ½ + *y*, ½ - *z*
C11	H11	S1	0.95	2.84	3.441(2)	122	-*x*, ½ + *y*, ½ - *z*
C14	H14	O4	0.95	2.47	3.159(2)	130	-*x*, 1 - *y*, -*z*
C19	H19b	S4	0.99	2.51	3.135(3)	121	-*x*, ½ + *y*, ½ - *z*
C3	H3c	Cg(N1,C7-C11)	0.98	2.98	3.908(3)	158	*x*, *y*, *z*
C1	S2	Cg(N1,C7-C11)	1.650(2)	3.533(1)	5.002(2)	147	1 - *x*, ½ + *y*, ½ - *z*
2							
C19	H19	Cg(Zn,S1,C1,S2)	0.95	2.74	3.149(2)	115	*x*, *y*, *z*

The overall two-dimensional fingerprint plots for **1** and **2** are presented in Figure 10a, and those delineated into explicit H···H, O···H/H···O, S···H/H···S and C···H/H···C contacts [52], focussing on specific pairwise interactions, are illustrated in Figures 10b-e, respectively; the percentage contributions from the different interatomic contacts to their Hirshfeld surfaces are summarised in Table 6. The greatest percentage contributions to the Hirshfeld surfaces of **1** and **2** are 41.1 and 48.5%, respectively, and arise from H···H contacts, Figure 10b, and indicate the prevalence of dispersive forces upon the packing. The fingerprint plot for **1** delineated into O···H/H···O contacts, Figure 10c, show a pair of long arrow spikes with their tips at $d_e + d_i \sim 2.1$ Å, these result from conventional N–H···O hydrogen bonding. Whereas in the case of **2**, and as summarised in Table 3, the pair of short broad spikes with tips at $d_e + d_i \sim 2.5$ Å result from C–H···O contacts. The distribution points in the fingerprint plot delineated into S···H/H···S contacts for both **1** and **2**, Figure 10d, characterise the N–H···S hydrogen bonds, Table 3, and the short interatomic S···H/H···S contacts, Tables 4 and 5. Thus, the conventional N–H···S hydrogen bonds in **1** and **2** are evident as the pair of forceps-like tips at $d_e + d_i \sim 2.8$ Å and ~ 2.4 Å, respectively. The short interatomic C–H···S contacts in crystals of **1** and **2** are viewed as the pair of green points in regions aligned from $d_e + d_i \sim 2.8$ Å in the donor and acceptor region of their respective plots. It is evident from the fingerprint plots delineated into C···H/H···C contacts, Figure 10e, that the significant 11.7% contribution from these contacts to the Hirshfeld surface of **1** has little influence upon the packing with separations greater than the sum of the van der Waals radii. On the other hand, the 10.0% contribution to the Hirshfeld surface of **2** results from the C–H···π contact involving the methylene-C7–H atom interacting with the N1-pyridyl ring, Table 3; the donors and acceptors of this interaction are highlighted in Figures 9b and c with blue and red circles, respectively.

Tab. 6: Percentage contributions of various intermolecular contacts to the Hirshfeld surfaces of **1** and **2**.

Contact	% contribution	
	1	**2**
H···H	41.1	48.5
O···H/H···O	13.7	10.5
S···H/H···S	23.4	25.6
C···H/H···C	11.7	10.0
N···H/H···N	1.8	2.7
C···S/S···C	3.3	0.4
N···Zn	1.5	0.0
N···S/S···N	0.9	0.0
S···S	0.7	0.4
Zn···H/H···Zn	0.6	0.3
N···O/O···N	0.5	0.0
C···C	0.5	0.0
C···O/O···C	0.2	0.6
S···O/O···S	0.0	1.0

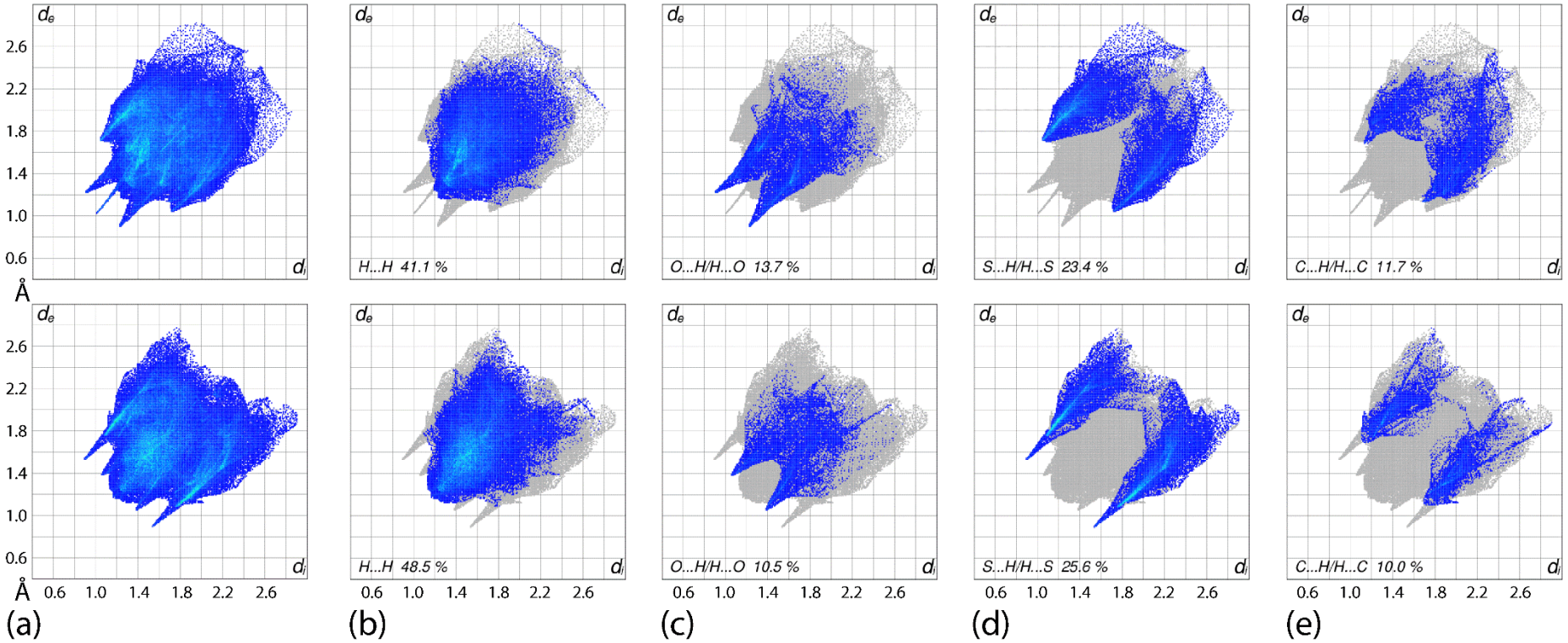

Fig. 10: Fingerprint plots calculated for **1** (upper plots) and **2**: (**a**) overall plots, and plots delineated into (**b**) H···H, (**c**) O···H/H···O, (**d**) S···H/H···S and (**e**) C···H/H···C contacts.

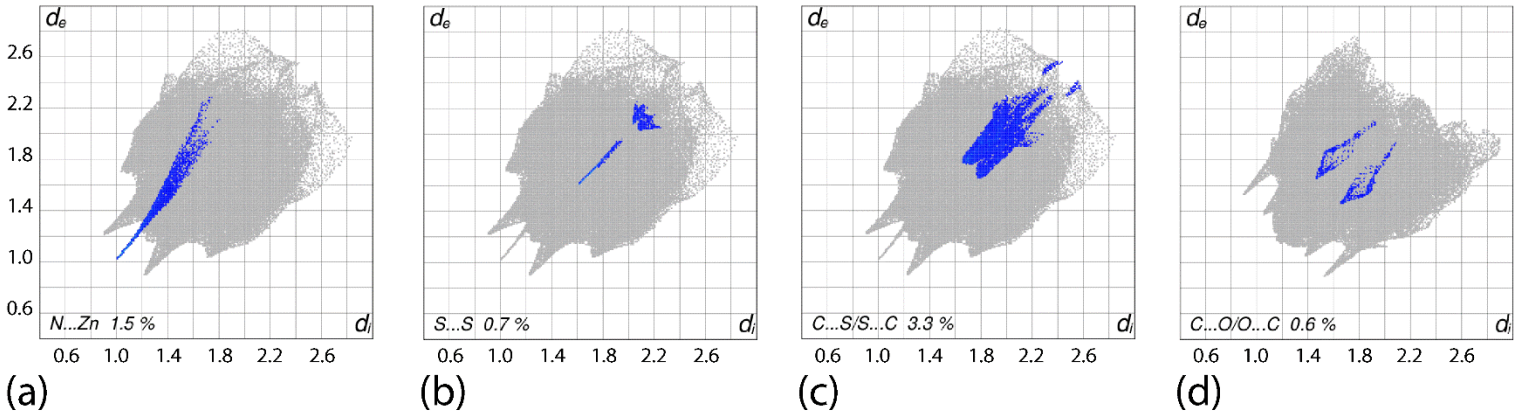

Fig. 11: Fingerprint plots delineated into: (**a**) **1**: N···Zn/Zn···N (**b**) **1**: S···S, (**c**) **1**: C···S/S···C and (**d**) **2**: C···O/O···C contacts.

Distinctive features of the delineated fingerprint plots for **1** and **2** are highlighted in Figure 11. The fingerprint plot delineated into N···Zn contacts for **1**, Figure 11a, presenting a thin long spike at $d_e + d_i \sim 2.0$ Å arises from the formation of the coordination polymer via Zn–N(pyridyl) bonds. The significance of the short interatomic S···S contacts in **1**, Table 4, is evident from the fingerprint plot in Figure 11b, specifically as the line segment beginning at $d_e + d_i \sim 3.2$ Å. Also, the presence of the C–S2···π(pyridyl) contact in the crystal of **1** is reflected in the fingerprint plot delineated into C···S/S···C contacts, Figure 11c. In the fingerprint delineated into C···O/O···C contacts showing a 0.6% contribution to the Hirshfeld surface of **2**, Figure 11d, the short interatomic C19···O1 contact, Table 4, is viewed as the pair of forceps-like short tips at $d_e + d_i \sim 3.1$ Å. The small contributions from the remaining interatomic contacts summarised in Table 4 have a negligible effect on the packing in the respective crystals.

Conclusions

The steric bulk of the oxygen-bound R group in $Zn(S_2COR)_2$ proved to be crucial in dictating the formation of a coordination polymer or not with $^4LH_2$ as the bridging ligand. Thus, for comparatively small R = Et, a twisted chain is generated (**1**) but when bulky R = Cy is present, a binuclear species is formed instead (**2**). These considerations also pertain supramolecular aggregation whereby conventional hydrogen bonding, i.e. both N–H···O and N–H···S, predominates in the crystal of **1**, leading to a three-dimensional architecture. By contrast, with bulky cyclohexyl groups in **2**, only N–H···S hydrogen bonding persists, leading to a supramolecular chain. This study shows that remote organic substituents are not necessarily innocent and can indeed be exploited to control the formation of coordination polymers.

Acknowledgments: We thank Sunway University for support of crystal engineering studies of metal 1,1-dithiolates.

References

[1] P. J. Heard, *Prog. Inorg. Chem.* **2005**, *53*, 1.
[2] G. Hogarth, *Prog. Inorg. Chem.* **2005**, *53*, 71.
[3] E. R. T. Tiekink, I. Haiduc, *Prog. Inorg. Chem.* **2005**, *54*, 127.
[4] I. Haiduc, D. B. Sowerby, *Polyhedron*, **1996**, *15*, 2469.
[5] E. R. T. Tiekink, *CrystEngComm*, **2003**, *5*, 101.
[6] E. R. T. Tiekink, *CrystEngComm*, **2006**, *8*, 104.
[7] E. R. T. Tiekink, *Coord. Chem Rev*. **2017**, *345*, 209.
[8] C. S. Lai, Y. X. Lim, T. C. Yap, E. R. T. Tiekink, *CrystEngComm*, **2002**, *4*, 596.
[9] E. R. T. Tiekink, *Crystals* **2018**, *8*, article no. 18.
[10] M. M. Jotani, P. Poplaukhin, H. D. Arman, E. R. T. Tiekink, *Acta Crystallogr. E* **2016**, *72*, 1085.
[11] R. F. Klevtsova, L. A. Glinskaya, E. I. Berus, S. V. Larionov, *J. Struct. Chem*. **2001**, *42*, 639.
[12] C. S. Lai, E. R. T. Tiekink, *Appl. Organomet. Chem*. **2003**, *17*, 251.
[13] D. Chen, C. S. Lai, E. R. T. Tiekink, *CrystEngComm* **2006**, *8*, 51.
[14] R. F. Klevtsova, T. G. Leonova, L. A. Glinskaya, S. V. Larionov, *Russ. J. Coord. Chem*. **2000**, *26*, 172.
[15] J.-G. Kang, J.-S. Shin, D.-H. Cho, Y.-K. Jeong, C. Park, S. F. Soh, C. S. Lai, E. R. T. Tiekink, *Cryst. Growth Des*. **2010**, *10*, 1247.
[16] I. Ara, F. El Bahij, M. Lachkar, *Synth. React. Inorg. Met.-Org. Nano-Met. Chem*. **2006**, *36*, 399.
[17] S. V. Larionov, L. A. Glinskaya, T. G. Leonova, R. F. Klevtsova, *Russ. J. Coord. Chem*. **1998**, *24*, 851.
[18] E. R. T. Tiekink, Crystal chemistry of the isomeric N,N'-bis(pyridin-n-ylmethyl)-ethanediamides, n = 2, 3 or 4. In: *Multi-Component Crystals:*

Synthesis, Concepts, Function (Eds. E. R. T. Tiekink and J. Schpector-Zukerman), De Gruyter, Singapore, **2017**.
[19] T. L. Nguyen, A. Scott, B. Dinkelmeyer, F. W. Fowler, J. W. Lauher, *New J. Chem*. **1998**, *22*, 129.
[20] N. S. Goro, S. M. Curtis, J. A. Webb, F. W. Fowler, J. W. Lauher, *Org. Lett*. **2005**, *7*, 1891.
[21] Q. Zeng, M. Li, D. Wu, S. Lei, C. Liu, L. Piao, Y. Yang, S. An, C. Wang, *Cryst. Growth Des*. **2008**, *8*, 869.
[22] P. Poplaukhin, E. R. T. Tiekink, *CrystEngComm* **2010**, *12*, 1302.
[23] H. D. Arman, P. Poplaukhin and E. R. T. Tiekink, *Acta Crystallogr. E* **2017**, *73*, 1501.
[24] H. D. Arman, P. Poplaukhin and E. R. T. Tiekink, *Z. Kristallogr. NCS* **2018**, *233*, 159.
[25] T. L. Nguyen, F. W. Fowler, J. W. Lauher, *J. Am. Chem. Soc*. **2001**, *123*, 11057.
[26] CrysAlis PRO, Rigaku Oxford Diffraction, Yarnton, Oxfordshire, England, 2017.
[27] G. M. Sheldrick, *Acta Crystallogr. A* **2008**, *64*, 112.
[28] G. M. Sheldrick, *Acta Crystallogr. C* **2015**, *71*, 3.
[29] L. J. Farrugia, *J. Appl. Crystallogr*. **2012**, *45*, 849.
[30] A. L. Spek, *J. Appl. Crystallogr*. **2003**, *36*, 7.
[31] K. Brandenburg, DIAMOND. Crystal Impact GbR, Bonn, Germany, **2006**.
[32] A. Bondi, *J. Phys. Chem*. **1964**, *68*, 441.
[33] L. Yang, D. R. Powell, R. P. Houser, *Dalton Trans*. **2007**, 955.
[34] G.-H, Lee, H. T. Wang, *Acta Crystallogr. C* **2007**, *63*, m216.
[35] G.-H. Lee, *Acta Crystallogr C* **2010**, *66*, o241.
[36] A. W. Addison, T. N. Rao, J. Reedijk, J. van Rijn, G. C. Verschoor, *J. Chem. Soc. Dalton Trans*. **1984**, 1349.
[37] C. S. Lai, S. Liu, E. R. T. Tiekink, *CrystEngComm* **2004**, *6*, 221.
[38] C. S. Lai, E. R. T. Tiekink, *CrystEngComm* **2004**, *6*, 593.
[39] D. Chen, C. S. Lai, E. R. T. Tiekink, *CrystEngComm* **2006**, *8*, 51.
[40] M.A. Buntine, M.J. Cox, Y.X. Lim, T.C. Yap, E.R.T. Tiekink, *Z. Kristallogr.* **2003**, *218*, 56.
[41] B.-C. Tzeng, Y.-C. Huang, B.-S. Chen, W.-M. Wu, S.-Y. Lee, G.-H. Lee, S.-M. Peng, *Inorg. Chem*. **2007**, *46*, 186.
[42] N. S. Goro, S. M. Curtis, J. A. Webb, F. W. Fowler, J. W. Lauher. *Org. Lett*. **2005**, *7*, 1891.
[43] T. L. Nguyen, A. Scott, B. Dinkelmeyer, F. W. Fowler, J. W. Lauher, *New J. Chem*. **1998**, *22*, 129.
[44] R. Custelcean, *Chem. Commun*. **2008**, 295.
[45] M. K. Corpinot, R. Guo, D. A. Tocher, A. B. M. Buanz, S. Gaisford, S. L. Price, D.-K. Bučar, *Cryst. Growth Des*. **2017**, *17*, 827.
[46] H. Biswal, Hydrogen Bonds Involving Sulfur: New Insights from ab Initio Calculations and Gas Phase Laser Spectroscopy. In: Scheiner S. (eds) Noncovalent Forces. Challenges and Advances in Computational Chemistry and Physics, vol 19. Springer, Cham, **2015**.
[47] J. J. McKinnon, M. A. Spackman, A. S. Mitchell, *Acta Crystallogr. B* **2004**, *60*, 627.
[48] S. K. Wolff, D. J. Grimwood, J. J. McKinnon, M. J. Turner, D. Jayatilaka, M. A. Spackman, Crystal Explorer (Version 3.1), University of Western Australia, **2012**.
[49] M. M. Jotani, Y. S. Tan, E. R. T. Tiekink, *Z. Kristallogr.* **2016**, *231*, 403.
[50] M. M. Jotani, P. Poplaukhin, H. D. Arman, E. R. T. Tiekink, *Z. Kristallogr.* **2017**, *232*, 287.
[51] Y. S. Tan, S. N. A. Halim, K. C. Molloy, A. L. Sudlow, A. Otero-de-la-Roza, E. R. T. Tiekink, *CrystEngComm* **2016**, *18*, 1105.
[52] J. J. McKinnon, D. Jayatilaka, M. A. Spackman, *Chem. Commun*. **2007**, 3814.